Supplementary Information to:
Antarctic temperature and global sea level closely coupled over the last five glacial cycles

Rohling, E.J., Grant, K., Bolshaw, M., Roberts, A.P., Siddall, M., Hemleben, Ch., and Kucera, M.

This *Supplementary Information* (*SI*) consists of 4 parts. Part 1 provides details and plots of several important relationships discussed in the main text. Part 2 discusses the development of a chronology for the Red Sea sea-level reconstructions. Part 3 provides a justification for the type of function used to fit the sea-level versus Antarctic Temperature anomaly data pairs derived in the paper. Part 4 concerns sensitivity tests to evaluate the robustness of the exponential fit function presented in main-text Figure 2b.

Part 1. Details and plots of important relationships discussed in the main text

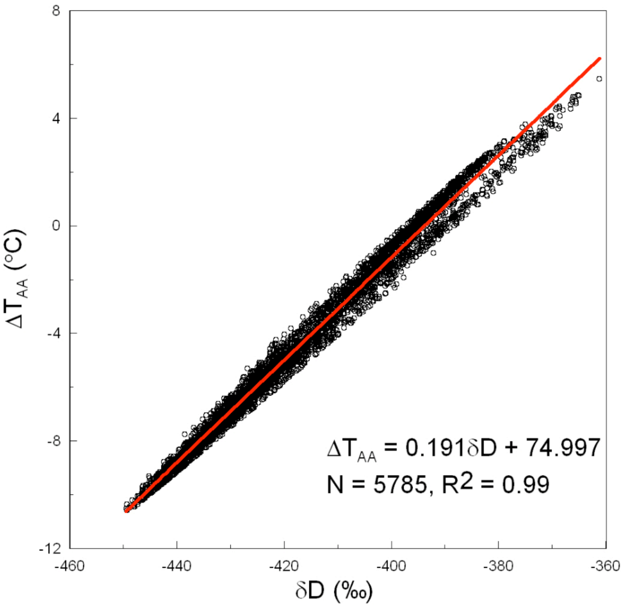

Figure S1. Antarctic Temperature anomaly (ΔT_{AA}) relative to the mean temperature of the last 1000 years, versus the stable hydrogen isotope values of ice in the EPICA Dome C ice core (Jouzel et al., 2007). This relationship was not plotted in the original publication, but the publicly available data files allow the simple regression plot to be reproduced and the fit statistics to be determined. The relationship used is closely approximated by a linear transformation.

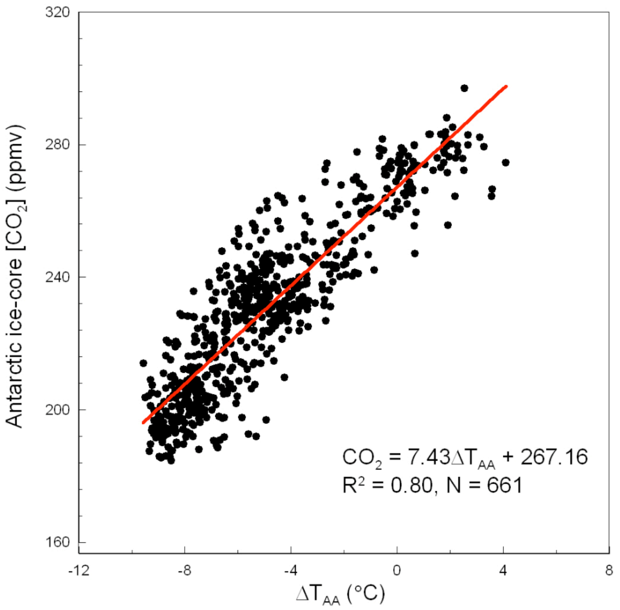

Figure S2. Regression plot between Antarctic Temperature anomaly (Jouzel et al., 2007) and CO_2 concentrations (Siegenthaler et al., 2005). This optimum correlation shown between $[CO_2]$ and ice δD given uncertainties in the ice-age to gas-age comparison in Antarctic ice cores reproduces that previously presented by Siegenthaler et al. (2005). The regression equation from Figure S2 is used in Figure 2 of the main text.

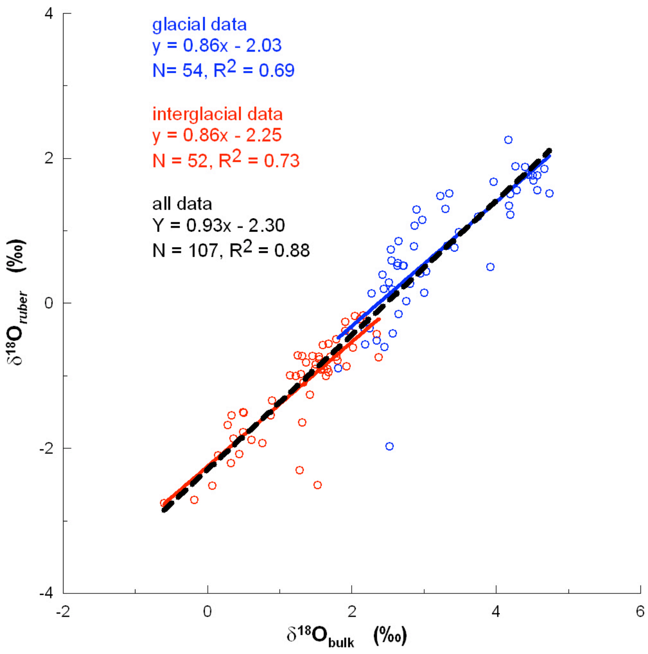

Figure S3. Relationship used to transform KL09 $\delta^{18}O_{bulk}$ into $\delta^{18}O_{ruber}$ equivalent values. Red and blue points (with linear regressions) indicate data for interglacial and glacial periods, respectively. The black dashed line represents a linear regression through all data points.

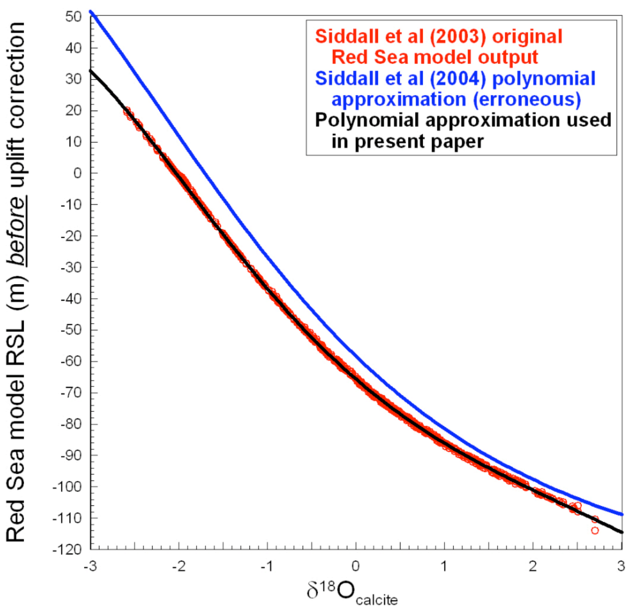

Figure S4. Original Red Sea model RSL data from Siddall et al (2003), as applied to $\delta^{18}O_{ruber}$ in central Red Sea sediment core GeoTü-KL11, compared with approximate polynomial fits (red). The blue line is the fit approximation that was previously published (Siddall et al., 2004). We found that its derivation contains an error, in that it was based on data in which a double correction was made for vital effect offsets in $\delta^{18}O_{ruber}$ through the high-resolution Holocene sequence, prior to regressing the values against model-derived RSL of Siddall et al. (2003). We have removed this double correction, and then compare the values with non-uplift corrected RSL values from the original model (red points). We then determined a best-fit 5th-order polynomial function (as in Siddall et al., 2004), which is represented by the black line. This new equation takes the form: $RSL_{(pre\ uplift\ correction)} = 0.0249\delta^{18}O_{ruber}^{5} - 0.1767\delta^{18}O_{ruber}^{4} - 0.2371\delta^{18}O_{ruber}^{3} + 4.3404\delta^{18}O_{ruber}^{2} - 24.424\delta^{18}O_{ruber} - 65.596$. The 5th-order polynomial form is not selected on statistical grounds, but is selected to approach as close as possible the form of the modelled relationship, taking into account the shape of the critical function, which describes changes in the strait cross-section with depth (Siddall et al., 2003, 2004). Note that the RSL values in Siddall et al. (2003, 2004) were obtained from their full model and are not affected; only the polynomial fit function they presented was erroneous. Isostatic effects are implicitly considered in the Siddall et al. (2003, 2004) calibration by its consideration of a scaling of the full LGM-Holocene sea-level amplitude to that observed in coral data (see elaboration of isostatic impacts based on ICE-5G in Siddall et al., 2004), and this Red Sea-based interpretation of global sea-level change was validated by full numerical solutions that comprehensively include isostacy (Biton et al., 2008).

Part 2. EDC3 chronology for RSL*

The depth-to-age transformation developed for core KL09 based on (manual) graphic correlation between the continuous $\delta^{18}O_{bulk}$ series (Figure S5b) and the Antarctic Temperature anomaly (ΔT_{AA}) record (Jouzel et al., 2007) is shown in Figure S5a (an identical routine was followed to place the combined KL11/MD92-1017 record on the EDC3 chronology). The tie-lines in Figure S5c are used to correlate depth in the core (top X-axis) to EDC3 age (bottom X-axis). The depth to age conversion is close to linear (Figure S5a), which implies a steady sedimentation rate, except between about 14 and 16m. This is the same stratigraphic interval as that where the EDC3 chronology was found (Parennin et al., 2007) to have a larger than expected offset from the orbitally tuned benthic isotope chronology of Lisiecki and Raymo (2004). We maintained correlation to the EDC3 chronology to facilitate direct comparison between our data and ΔT_{AA}, but the chronology through this interval clearly is a good target for further study.

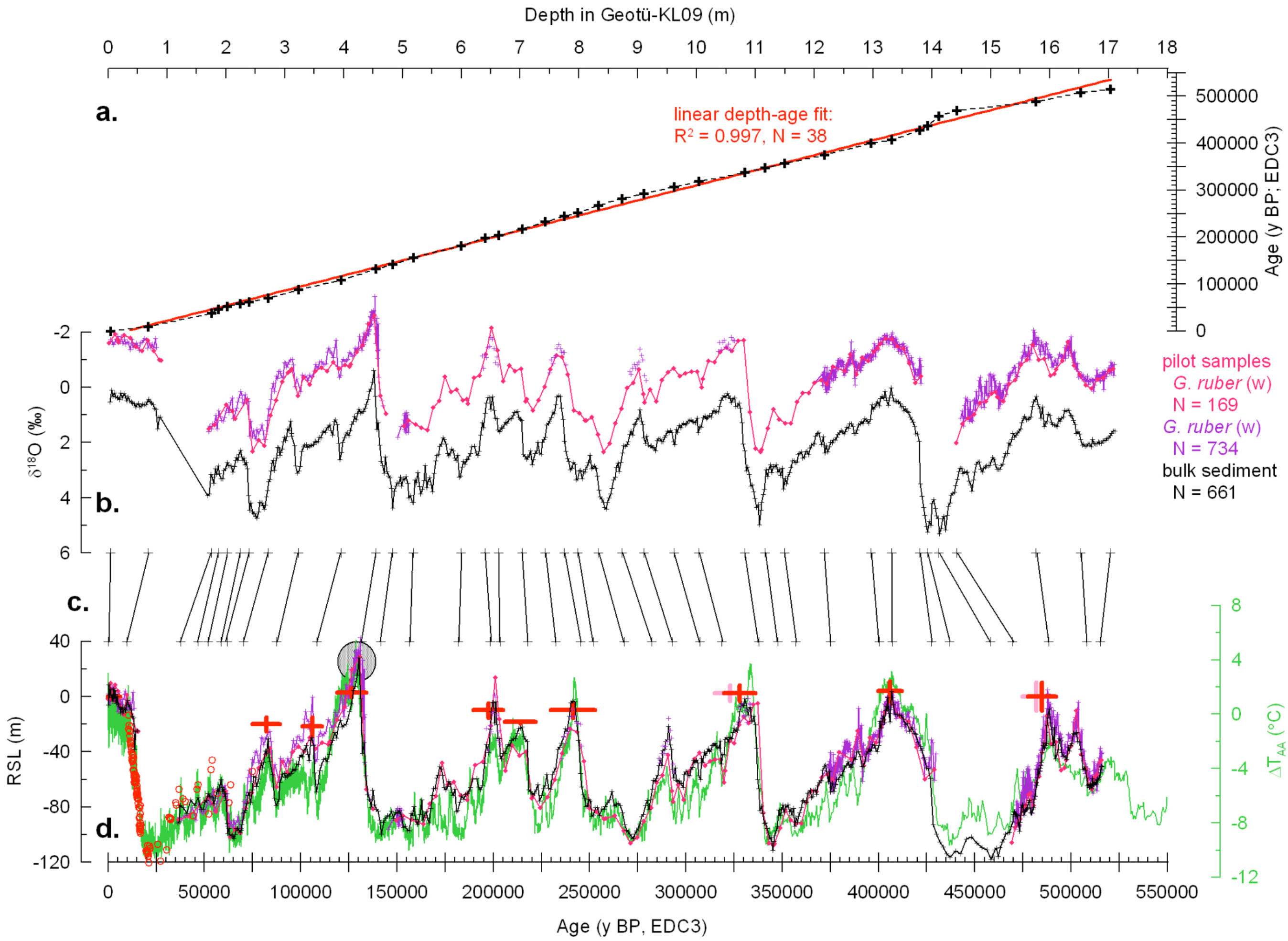

Figure S5. Results for central Red Sea core GeoTü-KL09: **a.** depth to age conversion; **b.** $\delta^{18}O_{bulk}$, high-resolution $\delta^{18}O_{ruber}$, and pilot-sample $\delta^{18}O_{ruber}$ (Rohling et al., 2008) versus depth in core; **c.** manually selected tie-lines used in graphic correlation between $\delta^{18}O_{bulk}$ and the Antarctic Temperature anomaly record (Jouzel et al., 2007) (green, in d) for conversion of depth in KL09 to the EPICA Dome C timescale 3 (EDC3) (Parennin et al., 2007); **d.** relative sea level (RSL) reconstructions based on the KL09 $\delta^{18}O$ data (colour as in b), versus age on the EDC3 timescale, compared with the Antarctic Temperature anomaly (ΔT_{AA}) record (Jouzel et al., 2007) (green). Clear outlier data within the hatched circle are discussed in the main text and *Methods*.

In red in Figure S5d, we show U-Th-dated coral and speleothem based sea-level data (after Siddall et al., 2003, 2006; Dutton et al., 2009). We have added +2 ky to the ages for these points, to make them comparable to the EDC3 chronology (see discussion/justification below). The coral and speleothem data corroborate the general amplitude of RSL variations, as well as the EDC3-based ages for previous interglacial maxima. Only for interglacial stages 9 and 13 (about 330 and 480 ky) do small discrepancies in the interglacial ages appear, and we 'compensate' for these by some minor additional adjustment (light red to dark red symbol shift) that remains within the combined age uncertainties.

Our systematic shifting of the U-Th-dated coral and speleothem data from their original chronology by addition of 2 ky follows the same philosophy as the routine applied in the original EDC3 paper when comparing with orbitally tuned benthic oxygen isotope data (Parennin et al., 2007). It negates any (likely) lag between ΔT_{AA} and the sea-level data. Unfortunately, the magnitude of that lag is well-established only for the last deglaciation, and not throughout the record (notably, not for the smaller sea-level fluctuations or for periods of increasing glaciation: for the variability between 65 and 45 ky, recent work suggests that RSL* and ΔT_{AA} coincide within the centennial-scale temporal uncertainties of methane synchronisation between Antarctic and Greenland ice-core records (Rohling et al., 2008)). A sharp, temporally distinct aeolian dust peak is recorded in magnetic susceptibility for KL09 after the Last Glacial Maximum aplanktonic zone, centered on 85 cm depth in the core – this is a likely expression of the Younger Dryas (Rohling et al., 2008). On our EDC3 timescale for KL09, the age for this level is about 14 ky, which in absolute terms is about 2 ky too old for the Younger Dryas. This corroborates our inference that the ΔT_{AA}-based EDC3 ages we have derived for the RSL* reconstruction may be too old by about 2 ky.

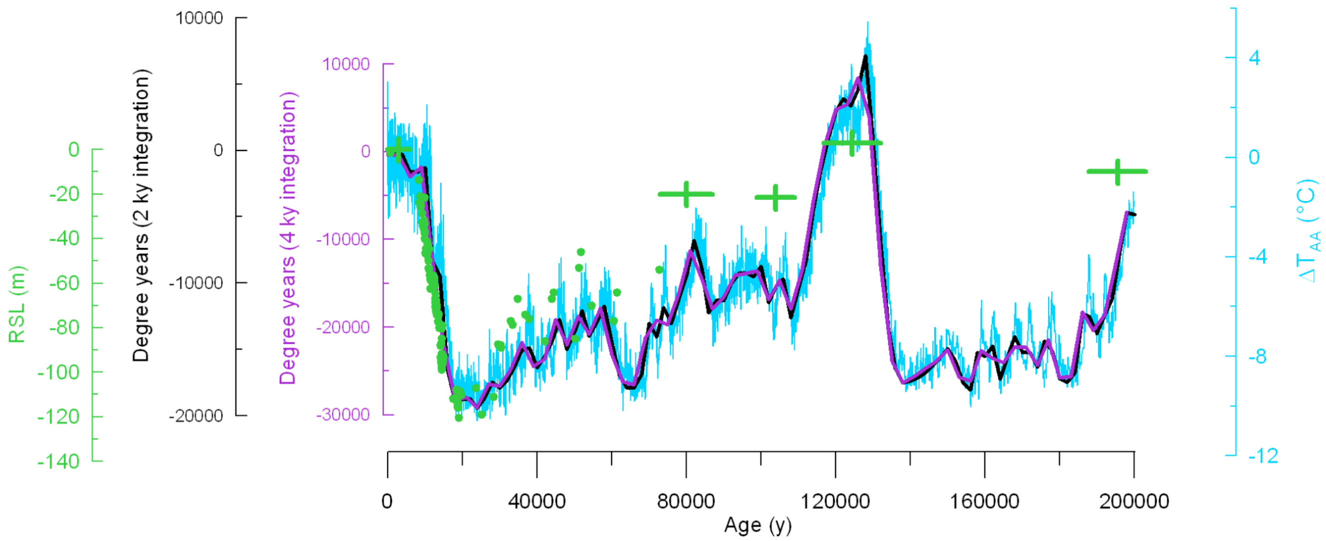

Figure S6. Chronological comparison between ΔT_{AA} (blue), 2 ky (black) and 4 ky (purple) integrations of ΔT_{AA}, and coral and speleothem-based RSL data (U-Th dated, using their original datings without adjustments). The records plot the integration with time of ΔT_{AA} over the preceding 2 ky (black) and 4 ky (blue); hence the units are given as degree years. This illustrates the time-integrated thermal gain/loss to which ice sheets may have responded (instead of the instantaneous ΔT_{AA} value).

The 2-4 ky integrations of the ΔT_{AA} record (giving data in degree years of thermal gain/loss) present a temporal variability that is very close to the original U-Th-dated values of the corals and speleothems at the last deglaciation (Figure S6). This offers further support our view that addition of +2 ky to the coral and speleothem ages is warranted for the purposes of comparison with ΔT_{AA} (and RSL*, which we synchronized to ΔT_{AA}). If it can be established that this integration period always involved a similar timescale, then the RSL* chronology may accordingly be shifted to younger values, which brings it into agreement with the original coral and speleothem U-Th ages and gives a good date for the Younger Dryas aeolian dust maximum in KL09. We suspect, however, that the integration timescale may depend on the 'type' of ice-volume change, making it different for deglaciations, small fluctuations, and glacial inceptions (see above). We did not want to introduce spurious chronological artefacts from uncertain assumptions, and therefore refrained from such involved and uncertain absolute 'tuning' of RSL* to ΔT_{AA}. Instead, we focus on the optimum (lagged) correlation, which is similar to the approach followed in correlating between ice-core hydrogen isotope (ice) and CO_2 (gas bubbles) fluctuations (Siegenthaler et al., 2005). We emphasize that our study is not aimed at resolving processes on millennial or shorter scales, which would require a better absolute chronology.

Part 3. Justification for exponential function through the ΔT_{AA}:RSL data

We use an exponential function to regress our observations, to take into account reduced sensitivity of ice volume to temperature at high temperature and sea level. Upon visual inspection, it is immediately clear that RSL* – and also its individual component datasets – displays a curvilinear trend when plotted against ΔT_{AA} (see main-text Figure 2, and also Figures S7, S8, S10), in agreement with the expected trajectories from modelling of ice-volume change relative to climate forcing (Pollard and DeConto, 2009). Although curvature might be accounted for using a simple polynomial function, there are restrictions to the shape of functions that are suitable for fitting sea-level/ice-volume versus temperature data, based on several well-established processes:

- Positive feedback processes induce rapid changes in the growth and retreat of ice sheets. First, surface albedo perturbations due to a change in area of ice cover (ice-albedo feedback) affects temperature in the vicinity of the ice sheet, which increases ice-sheet sensitivity to global temperature changes (Budyko, 1968; Sellers, 1969; North, 1984; Maqueda et al., 1998; Broccoli, 2000). Second, an increase (decrease) in ice-sheet area induced by a climate cooling (warming) causes the height/mass balance feedback, in which feedback between change in surface elevation and accumulation area induces changes in ice-sheet extent (Weertman, 1961, 1976; Pollard, 1980; Oerlemans, 1981; Abe-Ouchi and Blatter, 1993; Thompson and Pollard, 1997; DeConto and Pollard, 2003).
- Negative feedbacks become important at the extremely low sea levels associated with glacial maxima. First, increasing temperature towards the equator imposes meridional limits on ice-sheet growth, which restricts ice-sheets to higher latitudes. Accordingly, northern hemisphere ice sheets are known to have nucleated at high latitudes prior to expansion toward lower latitudes until some critical limit (Ives et al., 1975; Weertman, 1976; Pollard, 1980, 1983; Clark et al., 1993). Second, snow accumulation on ice sheets decreases at high elevations, which imposes a negative feedback on ice-sheet growth; the elevation-desert effect, which limits the height/mass balance feedback (Budd and Smith, 1979).

It is evident that, whatever function is used, it must account for an asymptotic trajectory toward high temperatures, at which no further melt is available. The asymptote value for total world ice volume lies in the region of +65 m. However, our ΔT_{AA}:RSL* relationship is validated only over the last 520 ky to 3.5 My, and so may be representative only for processes that do not include the main land-based East Antarctic Ice Sheet (EAIS) (see main text). In that case, the upper limit is less well known, and may be only a few metres above the Pliocene sea level of +25 m. We observe only limited hysteresis in our dataset (see main text, and *Part 4* below), and comparison with modelling results (Pollard and DeConto, 2009) therefore suggests that our relationship does not include EAIS processes. It was recently established that – where the southern hemisphere is concerned – Pliocene sea-level change was dominated by West Antarctic Ice Sheet fluctuations (Naish et al., 2009).

Key types of function that display a high-ΔT_{AA} asymptote as required are exponential, sigmoidal/logistic, rational, or inverse or hyperbolic trigonometric functions. Most of these follow a sigmoid pattern, but a sigmoid fit is not warranted in our case, because the lower end of the relationship is not adequately covered by our data. Although we acknowledge that a sigmoid function would allow reduced sensitivity of ice volume to temperature change at the lowest glacial temperatures (i.e., peak sea-level minima), (1) peak glacials are beyond the scope of the present paper, and (2) peak glacial periods are not ideally represented in stable isotope-based Red Sea sea-level records, because of aplanktonic conditions (Rohling et al., 1998; Fenton et al., 2000; Siddall et al., 2003) (see also below). Hence, it is better to use a function form that seeks only a high-ΔT_{AA} asymptote, which is why we use an exponential target curve for fitting through the data. A straightforward second-order polynomial fit through our ΔT_{AA}:RSL* data-set (with one apparent direction of curvature) would not asymptote, but would drop parabolically to low sea level at increasing ΔT_{AA}. This would clearly violate: (1) the expected (and previously modelled) trend of reducing ice volume for increasing warming; and (2) the Pliocene validation point (Figure S7).

In summary, the exponential relationship used limits the number of tunable parameters to a minimum, while constraining the behaviour of the fit outside of the tuning window (data cloud), in agreement with the deterministic feedbacks reviewed above. Second-order polynomial fitting is clearly inappropriate, and the use of higher order polynomials 'over-tunes' the regression and introduces unconstrained behaviour outside of the tuning window (Figure S7).

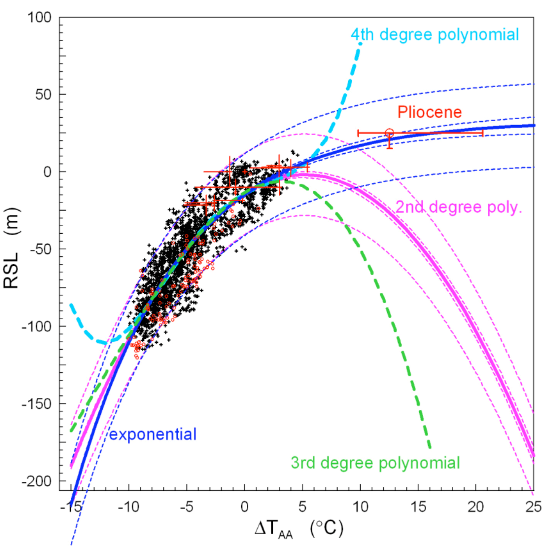

Figure S7. Reproduction of main-text Figure 2b, with the requested addition of polynomial fit functions: 2nd order polynomial fit function (magenta, with 95% confidence envelopes similar to those presented for the exponential fit (blue)); and 3rd and 4th order polynomials.

Finally, it is relevant to briefly discuss the issues with determining glacial RSL values below about –100 m with the $\delta^{18}O$-based Red Sea method. As mentioned above, the method suffers some weakness during those periods, because of the presence of hypersalinity-induced (S >49) aplanktonic conditions in the Red Sea (Rohling et al., 1998; Fenton et al., 2000; Siddall et al., 2003). As a consequence, RSL reconstructions presented in the present study for those intervals (notably MIS 2 and MIS 12, see *Part 4* below) rely on only bulk sediment-based values (main-text Figure 1) along with two roughly intercalibrated benthic foraminiferal values from KL11 (Siddall et al., 2003). The presence of abundant (inorganic and/or microbially mediated) carbonate cementation and overgrowths within the aplanktonic zones weakens the reliability of Red Sea RSL reconstructions for those intervals. This may (partially) explain why full glacial

RSL values found here suggest less sea-level lowering than those suggested by Rohling et al. (1998) based on Red Sea hypersalinity conditions as derived from faunal abundances and absence/presence arguments. However, note also that Rohling et al. (1998) employed very basic hydraulic control calculations for Bab-el-Mandab that considered only two layers, while the present study relies on the more realistic 3-layer model of Siddall et al. (2002), which also (partly) accounts for difference between glacial low-stand estimates from the two methods. In short, although Red Sea records provide rare insight into past full glacial sea-level low-stands, the uncertainties are clearly larger than in periods outside full glacial conditions (i.e., RSL above –100 m). Full corroboration has to await the advent of coral-based estimates for glacial low-stands prior to the Last Glacial Maximum, which as yet do not exist.

Part 4. Sensitivity analyses

We now investigate the preferred exponential fit function based on separate component data-sets within our total ΔT_{AA}:RSL dataset. The expectation should be that none of the fits would asymptote in excess of about +65 m at high ΔT_{AA}. As discussed above, this may already be too high a value, but as yet we do not know whether the relationship is valid also before 3.5 My or not. Regardless, the firm upper limit (within uncertainty) must be about +65 m. Figure S8 contains separate fits for the RSL data based on: KL09 $\delta^{18}O_{bulk}$ (Figure S8a), high-resolution KL09 $\delta^{18}O_{ruber}$ (Figure S8b), all high-resolution $\delta^{18}O_{ruber}$ data from KL09, KL11, and MD92-1017 (Figure S8c), all RSL data combined in this study including the outlier KL09 data for MIS-5e (Figure S8d) (see main text), and all RSL data combined in this study excluding the outlier KL09 data for MIS-5e (Figure S8e) (see main text). Figure 8f contains the fit for data after applying a 3-pt moving average (RSL*, green dashed fit line, which is the main fit in main-text Figure 2b) alongside the fit functions determined only for periods of sea-level rise (red) and periods of sea-level lowering (blue) (Figure S9 and fit statistics in Table S1). From these different permutations of our dataset, it is evident that the form of the exponential fit function is robust with respect to: (a) the individual selection of component datasets; (b) comparison between raw (Figures S8d and e) and averaged (RSL*, Figure S8f) data; and (c) inclusion or exclusion of the apparent outlier MIS-5e values from KL09. Also, there does not seem to be any large hysteresis in the dataset with respect to periods of waxing or waning ice volume – at least not on the millennial and larger timescales considered here (Figure 8f).

In Figure S10, we compare the fit functions for RSL* excluding (as main-text Figure 2b) and including the outlier KL09 MIS-5e data (circle). The fits are not identical, but very close, and illustrate that our conclusions are not significantly affected if the outlier values were retained. If anything, the conclusions appear to be based on conservative interpretation of the dataset. The RSL* reconstruction with excluded outliers (see main text) is in better agreement with the Pliocene validation point.

Finally, in Figure S11 we show the distribution of residuals of measured RSL* around an RSL* ‘simulation’ based on the exponential regression function (relative to ΔT_{AA}) developed in main-text Figure 2b. The residuals show no statistically significant bias in a positive or negative direction for glacial or interglacial periods (interglacials highlighted with pink bands). In addition, identification of the 1σ intervals for the residuals around the regression-based RSL* estimates through successive glacial cycles indicates that the residuals show no systematic bias in magnitude through time. This suggests that the ΔT_{AA}:RSL* regression performs the same for individual glacial cycles as for the overall record. Note that we focus on large-scale trends, and that for comparison (regressions) of more detailed subdivisions of the data, detailed synchronization issues between the Red Sea and ice-core records would become disproportionately important (in this current study, these detailed issues are part of the ‘noise’ around the regressions).

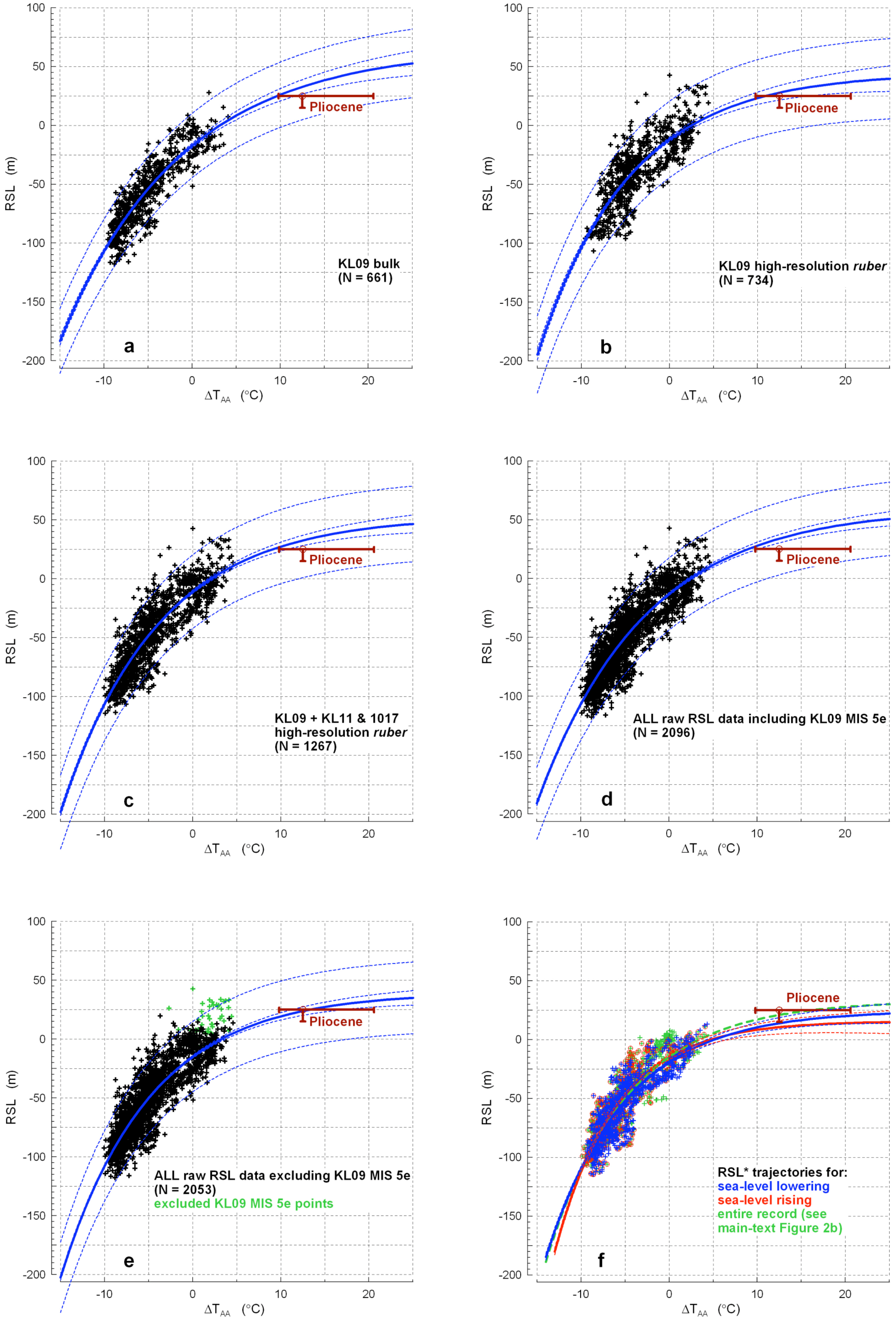

Figure S8. Sensitivity tests for the exponential fit function as discussed in this section. Details for the various fits are listed in Table S1.

Table S1. Fit parameters for regressions of relative sea level (RSL) and Antarctic temperature anomaly (ΔT_{AA}). All fit functions take the form $RSL = \alpha \cdot e^{\beta \cdot \Delta T_{AA}} + \gamma$. Final two columns indicate each fit function's RSL value at ΔT_{AA} = 16°C (the value predicted by extrapolation of the natural ΔT_{AA}:[CO_2] relationship to [CO_2] = 387 ppmv; main-text Fig. 2a), and the 95% confidence limit for the fit at that point. Red highlights the case portrayed in main text Fig 2b.

Parameter regressed against ΔT_{AA}	Sediment Core(s)	N	η^2	α	β	γ (= high ΔT_{AA} asymp-tote)	Fig.	fit RSL at ΔT_{AA} = 16°C	95% conf. margin of fit at ΔT_{AA} = 16
RSL_{bulk}	KL09	661	0.77	–83.176	–0.073	66.069	S8a	40.3	7.3
$RSL_{high\ res.\mathit{ruber}}$	KL09	734	0.66	–56.776	–0.096	44.994	S8b	32.8	7.5
$RSL_{all\ high\ res.\ \mathit{ruber}}$	KL09+KL 11+1017	1267	0.76	–64.190	–0.091	53.205	S8c	38.2	5.3
All raw RSL data (incl. KL09 MIS5e)	KL09+KL 11+1017	2096	0.75	–73.215	–0.082	60.164	S8d	40.5	4.2
RSL* (incl. KL09 MIS5e)	KL09+KL 11+1017	2095	0.80	–65.114	–0.090	52.474	S10	37.2	3.7
All raw RSL data (excl. KL09 MIS5e)	KL09+KL 11+1017	2053	0.74	–54.533	–0.099	39.652	S8e	28.5	4.3
RSL* (excl. KL09 MIS5e)	KL09+KL 11+1017	2052	0.79	–47.716	–0.110	33.045	1, 2 S8f S10	24.8	3.8
RSL* falling only	KL09+KL 11+1017	971	0.76	–43.900	–0.112	24.782	S8f	17.4	5.8
RSL* rising only	KL09+KL 11+1017	583	0.81	–30.598	–0.143	15.681	S8f	12.6	6.8

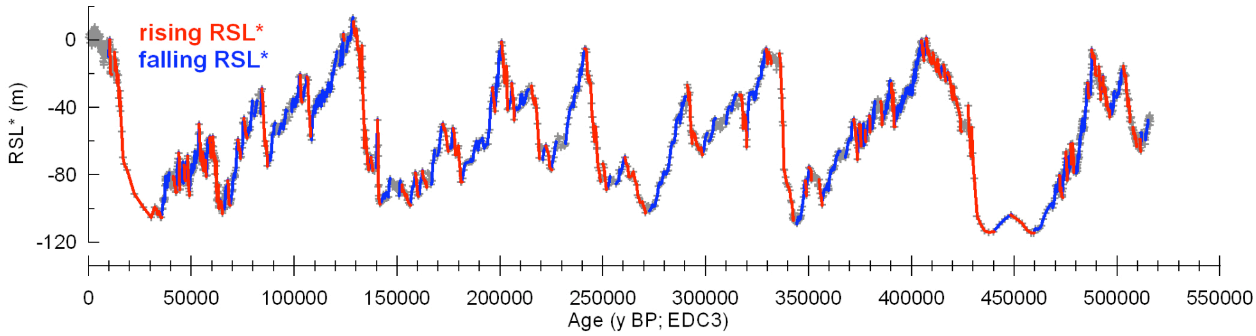

Figure S9. Identified sectors in RSL* where sea level dominantly rises (red) or falls (blue). These are the sectors that underlie the fit functions displayed in Figure S8f.

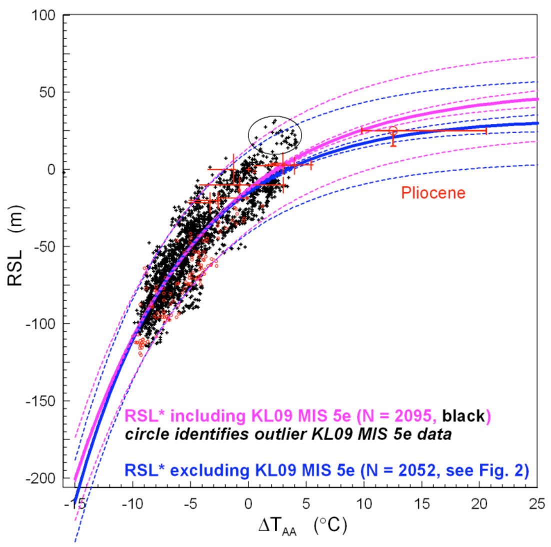

Figure S10. Reproduction of main-text Figure 2b, (blue fit and confidence margins), with the addition of the data (black), fit and confidence margins (magenta) for RSL* without exclusion of the outlier KL09 MIS 5e data. Details of the fits are listed in Table S1.

The only large difference between the regression-based RSL* model and the RSL* data (Figure S11) concerns the MIS 12 glacial (~ 475-425 ky). This interval should be interpreted with care, because MIS 12 is characterised by an aplanktonic zone with abundant carbonate cementation in the Red Sea (Rohling et al., 1998; Fenton et al., 2000), and because other indicators suggest that RSL for MIS 12 may have been even lower than indicated here (Rohling et al., 1998). This interval does not noticeably affect our conclusions because – for reasons explained in Part 3 of this supplement – this study is not primarily concerned with full glacial conditions.

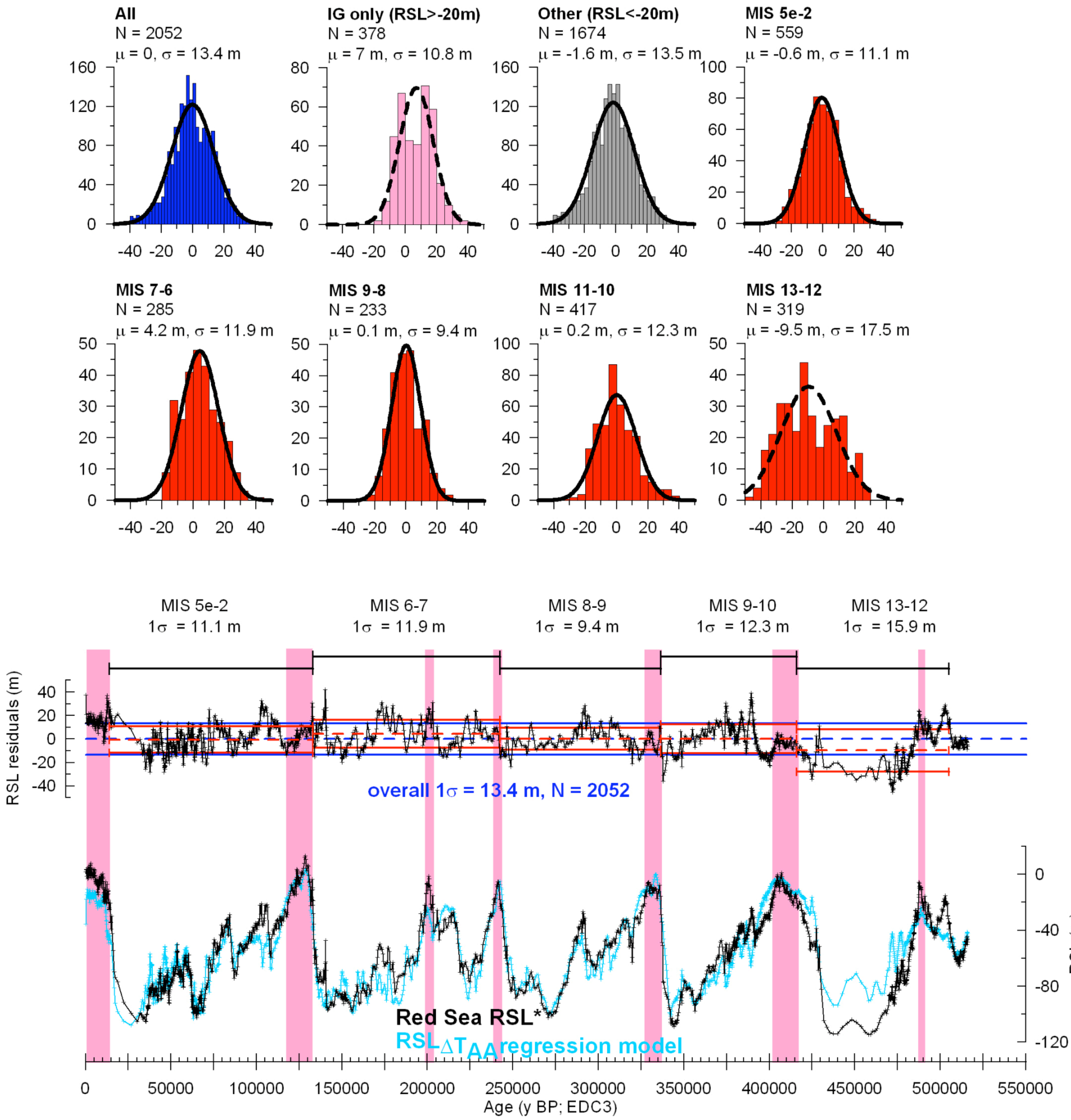

Figure S11. Residuals versus time for RSL* relative to RSL* estimates from the exponential relationship relative to ΔT_{AA} as developed in main-text Figure 2b. Pink zones identify interglacial intervals (arbitrarily identified where RSL* > –20 m). Histograms with Gaussian fit curves (dashed where poorly defined) are distributions of residuals for all data, interglacial (IG) data only, all non-IG ('other') data, and for individual glacial cycles. Red bars in the central panel indicate 1σ intervals (solid) and means (dashed) for the residuals in the successive glacial cycles, and blue bars indicate 1σ intervals (solid) and means (dashed) for the residuals in the entire dataset (based on the histograms).

References

Abe-Ouchi, A. & Blatter, H., On the initiation of ice sheets, *Ann. Glaciol.* **18**, 203-207 (1993).

Biton, E., Gildor, H. & Peltier, W.R., Relative sea level reduction at the Red Sea during the Last Glacial Maximum, *Paleoceanography* **23**, PA1214, doi:10.1029/ 2007PA001431 (2008).

Broccoli, A.J., Tropical cooling at the last glacial maximum: an atmosphere-mixed layer ocean model simulation, *J. Clim.* **13**, 951-976 (2000).

Budd, W.F. & Smith, I.N., The growth and retreat of ice sheets in response to orbital radiation changes, *Int. Assoc. Hydrol. Sci. Publ.* **131**, 369-409 (1979).

Budyko, M.I., The effect of solar radiation variations on the climate of the Earth, *Tellus* **21**, 611-619 (1969).

Clark, P.U., *et al.*, Initiation and development of the Laurentide and Cordilleran ice sheets following the last interglaciation, *Quat. Sci. Rev.* **12**, 79-114 (1993).

DeConto, R.M. & Pollard, D., A coupled climate-ice sheet modeling approach to the early Cenozoic history of the Antarctic ice sheet, *Palaeogeogr. Palaeoclimatol. Palaeoecol.* **198**, 39-52 (2003).

Dutton, A., *et al.*, Phasing and amplitude of sea-level and climate change during the penultimate interglacial, *Nat. Geosc.* **2**, 355-359 (2009).

Fenton, M., Geiselhart, S., Rohling, E.J., Hemleben, Ch., Aplanktonic zones in the Red Sea. *Mar. Micropaleontol.* **40**, 277-294 (2000).

Ives, J.D., Andreas, J.T. & Barry, R.G., Growth and decay of Laurentide ice sheet and comparisons with Fenno-Scandinavia, *Naturwissenschaften* **62**, 118-125, (1975).

Jouzel, J., *et al.*, Orbital and millennial Antarctic climate variability over the past 800,000 years. *Science* **317**, 793-796 (2007).

Lisiecki, L.E. & Raymo, M.E, A Plio-Pleistocene stack of 57 globally distributed benthic δ^{18}O records, *Paleoceanography* **20**, PA1003, doi:10.1029/ 2004PA001071, 2005.

Maqueda, M.A.M., Willmott, A.J., Bamber, J.L. & Darby, M.S., An investigation of the small ice cap instability in the Southern Hemisphere with a coupled atmosphere–sea ice–ocean–terrestrial ice model, *Clim. Dyn.* **14**, 329-352 (1998).

Naish, T. *et al.*, Obliquity-paced Pliocene West Antarctic ice sheet oscillations, *Nature* **458**, 322–328 (2009).

North, G.R., The small ice cap instability in diffusive climate models, *J. Atmos. Sci.* **41**, 3390-3395 (1984).

Oerlemans, J., Some basic experiments with a vertically integrated ice sheet model, *Tellus* **33**, 1-11 (1981).

Parrenin, F., *et al.*, The EDC3 chronology for the EPICA Dome C ice core, *Clim. Past* **3**, 485–497 (2007).

Pollard, D., A simple parameterization for ice-sheet ablation rate, *Tellus* **32**, 384-388 (1980).

Pollard, D., Ice-age simulations with a calving ice-sheet model, *Quat. Res.* **20**, 30-48 (1983).

Pollard, D. & DeConto, R.M., Modelling West Antarctic ice sheet growth and collapse through the past five million years, *Nature* **458**, 329–332 (2009).

Rohling, E.J., *et al.*, Magnitudes of sea-level lowstands of the past 500,000 years, *Nature* **394**, 162-165 (1998).

Rohling, E.J., *et al.*, New constraints on the timing and amplitude of sea level fluctuations during early to middle marine isotope stage 3, *Paleoceanography* **23**, PA3219, doi:10.1029/2008PA001617 (2008).

Sellers, W.D., A global climate model based on the energy balance of the earth-atmosphere system, *J. Appl. Meteorol.* **8**, 1972-1983 (1969).

Siddall M., Chappell J. & Potter E.K., Eustatic sea level during past interglacials, in: `*The climate of past interglacials*', Sirocko, F., Litt, T., Claussen, M. & Sanchez-Goni, M.F. (eds.), Elsevier, Amsterdam, pp. 75–92 (2006).

Siddall, M., Smeed, D., Mathiessen, S., and Rohling, E.J., Modelling the seasonal cycle of the exchange flow in Bab-el-Mandab (Red Sea), *Deep-Sea Res. I* **49**, 1551-1569 (2002).

Siddall, M., *et al.*, Sea-level fluctuations during the last glacial cycle, *Nature* **423**, 853-858 (2003).

Siddall, M., *et al.*, Understanding the Red Sea response to sea level, *Earth Planet. Sci. Lett.* **225**, 421-434 (2004).

Siegenthaler, U., *et al.*, Stable carbon cycle–climate relationship during the Late Pleistocene, *Science* **310**, 1313-1317 (2005).

Thompson, S.L. & Pollard D., Greenland and Antarctic mass balances for present and doubled atmospheric CO_2 from the GENESIS version-2 global climate model, *J. Clim.* **10**, 871-900 (1997).

Weertman, J., Stability of ice-age ice sheets, *J. Geophys. Res.* **66**, 3783-3792 (1961).

Weertman, J., Milankovitch solar radiation variations and ice age ice sheet sizes, *Nature* **261**, 17-20 (1976).